Regional ocean grid refinement and its effect on simulated atmospheric climate

Jonny Williams[1], Erik Behrens[1], Olaf Morgenstern[1], João Teixeira[2], Vidya Varma[1,3], and Wolfgang Hayek[1]

[1]National Institute of Water and Atmospheric Research (NIWA)
[2]Met Office
[3]Now at Institut für Geophysik und Meteorologie, Universität zu Köln

February 15, 2023

Abstract

In this work we show the effect on atmospheric climate of including a two-way-nested, high-resolution ocean model in the region surrounding New Zealand within a coupled earth system model. The resolution of the regional, nested ocean model is approximately 0.2 degrees compared to the 1 degree resolution of the global ocean model within which it is embedded and this work complements previously published work on ocean circulation and marine heatwaves using the New Zealand Earth System Model, NZESM. After a discussion of the eddy-permitting capability of the nested ocean and its coupling to the overlaying atmosphere, we study the effects on air temperature, precipitation and evaporation, latent and sensible surface heat balances, zonal and meridional winds, the anticyclonic storm track and the effect on clouds. With respect to clouds, we show that stratocumulus is found to be the most sensitive cloud type when partitioning the results by cloud-top-pressure and optical depth. Overall we find that the NZESM provides a better representation of regional atmospheric climate compared to its parent model - the UKESM - although this improvement is not universal. For example, although the NZESM shows better agreement in surface air temperature within the nested ocean region, there is also some deterioration in the agreement compared to the UKESM at high southern latitudes where the seasonal sea-ice edge coincides with a transition from negative to positive correlation between air temperature and cloud amount. The lack of additional model tuning in the NZESM after the nested ocean model's inclusion largely accounts for the presence of these improvement-deterioration pairs.

Regional ocean grid refinement and its effect on simulated atmospheric climate

Jonny Williams[1,*], Erik Behrens[1], Olaf Morgenstern[1], João Teixeira[2], Vidya Varma[1,3], and Wolfgang Hayek[1]

[1]*National Institute of Water and Atmospheric Research (NIWA), Hataitai, Wellington, New Zealand*
[2]*Met Office, Fitzroy Road, EX1 3PB, Exeter, UK*
[3]*Now at Institut für Geophysik und Meteorologie, Universität zu Köln, Pohligstraße 3, 50969 Köln, Germany*
[*]*Corresponding author: Jonny Williams, jonny.williams@niwa.co.nz*

February 13, 2023

Abstract

In this work we show the effect on atmospheric climate of including a two-way-nested, high-resolution ocean model in the region surrounding New Zealand within a coupled earth system model. The resolution of the regional, nested ocean model is approximately 0.2° compared to the 1° resolution of the global ocean model within which it is embedded and this work complements previously published work on ocean circulation and marine heatwaves using the New Zealand Earth System Model, NZESM. After a discussion of the eddy-permitting capability of the nested ocean and its coupling to the overlaying atmosphere, we study the effects on air temperature, precipitation and evaporation, latent and sensible surface heat balances, zonal and meridional winds, the anticyclonic storm track and the effect on clouds. With respect to clouds, we show that stratocumulus is found to be the most sensitive cloud type when partitioning the results by cloud-top-pressure and optical depth. Overall we find that the NZESM provides a better representation of regional atmospheric climate compared to its parent model – the UKESM – although this improvement is not universal. For example, although the NZESM shows better agreement in surface air temperature within the nested ocean region, there is also some deterioration in the agreement compared to the UKESM at high southern latitudes where the seasonal sea-ice edge coincides with a transition from negative to positive correlation between air temperature and cloud amount. The lack of additional model tuning in the NZESM after the nested ocean model's inclusion largely accounts for the presence of these improvement-deterioration pairs.

Keywords: Climate, Simulation, Validation

1 Introduction

Earth System Models - ESMs - are complex and computationally intensive pieces of software for understanding past climates and informing projections of future ones. A single simulation can use thousands of computer processors and can easily generate tens or hundreds of terabytes of data, e.g. [1].

The New Zealand Earth System Model - NZESM [2, 3] - is a modified version of the low-resolution configuration of the United Kingdom Earth System Model UKESM version 1.0 [4]. The physical oceanography of the NZESM is described in detail in [3]; the only difference to the UKESM is the inclusion of an embedded high-resolution ocean model in the New Zealand region. This is discussed in more detail below.

Climate models' representation of Southern Ocean climate is subject to some notable biases. The Southern Ocean warm bias is arguably the most prominent one, however, there are associated biases in cloud properties and - concomitantly - in their radiative effects [5, 6, 7].

Several authors have documented Southern Ocean model bias as well as the mechanisms that contribute to them [8, 9, 10]. For example, [8] demonstrated that Southern Ocean model-observation mismatches can be interpreted as being due to shortwave radiation biases in the clouds and surface radiation fields. [9] studied cloud microphysics – specifically the shape of ice crystals in the atmosphere – and find that relaxation of the traditional assumption of spherical crystals yields an improvement of up to 4 Wm^{-2}. In contrast, [10] study the effect on surface radiation biases due to cloud biases in cyclone systems, developing a new clustering method and concluding that the resulting biases are predominantly due to mid and low level clouds in the cold air sector of the cyclones.

The studies above consider atmosphere-only GCMs but ocean-only and coupled models have also been used to investigate Southern Ocean biases. It is beyond the scope of this work to give an exhaustive review of our understanding of the Southern Ocean biases present in coupled climate models; something that is persistent and widespread in coupled models from CMIP5 and CMIP6. The UKESM is a complex coupled earth system model, and its varied processes are documented across many publications.

Southern Ocean biases in coupled climate models are two-fold, manifesting in a persistent surface warm bias of the Southern Ocean (e.g. [11] §3.1) and in a large shortwave cloud radiative effect - SWCRE - bias in the same region (e.g. [9] §3). In coupled models these biases are inherently connected, and this study exhibits changes to both biases even though the atmosphere component in the two model configurations studied is identical.

For example, [12] examine the HadGEM2-ES coupled model, results from which were submitted to the 5^{th} Coupled Model Intercomparison Project (CMIP5) [13]. This study discusses the origin of the model's bias in detail and describes the effects of corrections to the albedo over the Southern Ocean on - for example - atmospheric jets and the 'double ITCZ' problem (e.g. see [14] for a review).

From the perspective of ocean-only models, [15] provides a detailed overview of the basis and findings of the second phase of the Ocean Model Intercomparison Project (OMIP2). More specifically, [16] and [17] examine the role of horizontal grid resolution with [16] finding that although some fields are consistently improved as resolution increases - western boundary, equatorial and Antarctic circumpolar currents - some are degraded in some models, e.g. temperature and salinity profiles.

2 Models and datasets

2.1 Model description

The atmospheric component of the models used here is the 'Global Atmosphere Model, Version 7.1' – GA7.1 [18] – configuration of the Unified Model, so-called due to its ability to simulate weather and climate in a unified way. It uses a semi-implicit semi-Lagrangian dynamical core [19], the SOCRATES radiation scheme, based on [20], shallow and deep mass-flux-based convection - e.g. [21] - and sub-gridscale boundary layer turbulence - e.g. [22]. The models also simulate explicit tropospheric and stratospheric chemistry [23].

Clouds are described by [24] and [25] and their inclusion into the atmospheric component of the UKESM is described in [18]. In this scheme, cloud condensate *and* cloud fraction are prognostic variables; that is, they are calculated 'online' within the equation system solved by the model code. This improves on the previous 'diagnostic' scheme used in weather and climate forecasting codes used by members of the Unified Model Partnership [26] by more realistically linking water vapour, condensate, and cloud fraction amounts.

The ocean model used is NEMO [27], which contains the MEDUSA ocean biogeochemistry simulator [28] and is coupled coupled to the sea ice model CICE [29]. The specific configuration used here – including a detailed description of the Southern Ocean – used by the models is documented in [30] and [11] and is known as 'Global Ocean Model, Version 6', or GO6. Compared to the previous iteration of the 'GO' family of models, GO6 shows multi-variable improvements in the Southern Ocean region which are attributed to changes in ocean mixing parameter values. The coupling between the different model components is done via the OASIS coupler, which is used in several CMIP6-standard models [31].

The physical basis model (coupled ocean-atmosphere-sea ice but without the full biogeochemical complexity) of the UKESM is called HadGEM3-GC31-LL [32]. This model exists in two resolutions, N96ORCA1 (the parent resolution of the NZESM) and N216ORCA025 and the former exhibits a smaller overall Southern Ocean warm bias due to improved volumetric ACC transport and a higher fidelity annual sea ice cycle. The overall UKESM climatology is described in [33].

2.2 Eddies and resolution mismatches

The configureation of the NZESM described here includes a two-way nested, high-resolution ocean version of the GO6 model in the New Zealand region whilst keeping all other aspects of the ocean model unchanged. This nesting has been achieved using the Adaptive Grid Refinement In Fortran – AGRIF – method [34] and has increased the nominal ocean grid resolution from 1° to 0.2°; thus achieving a 25 fold increase in areal mesh density. The physical oceanography of the UKESM/NZESM model pair is described in [3] and the nested region is illustrated in Figure 1. This study uses the same two simulations considered in [3] but analyses them from an atmospheric perspective.

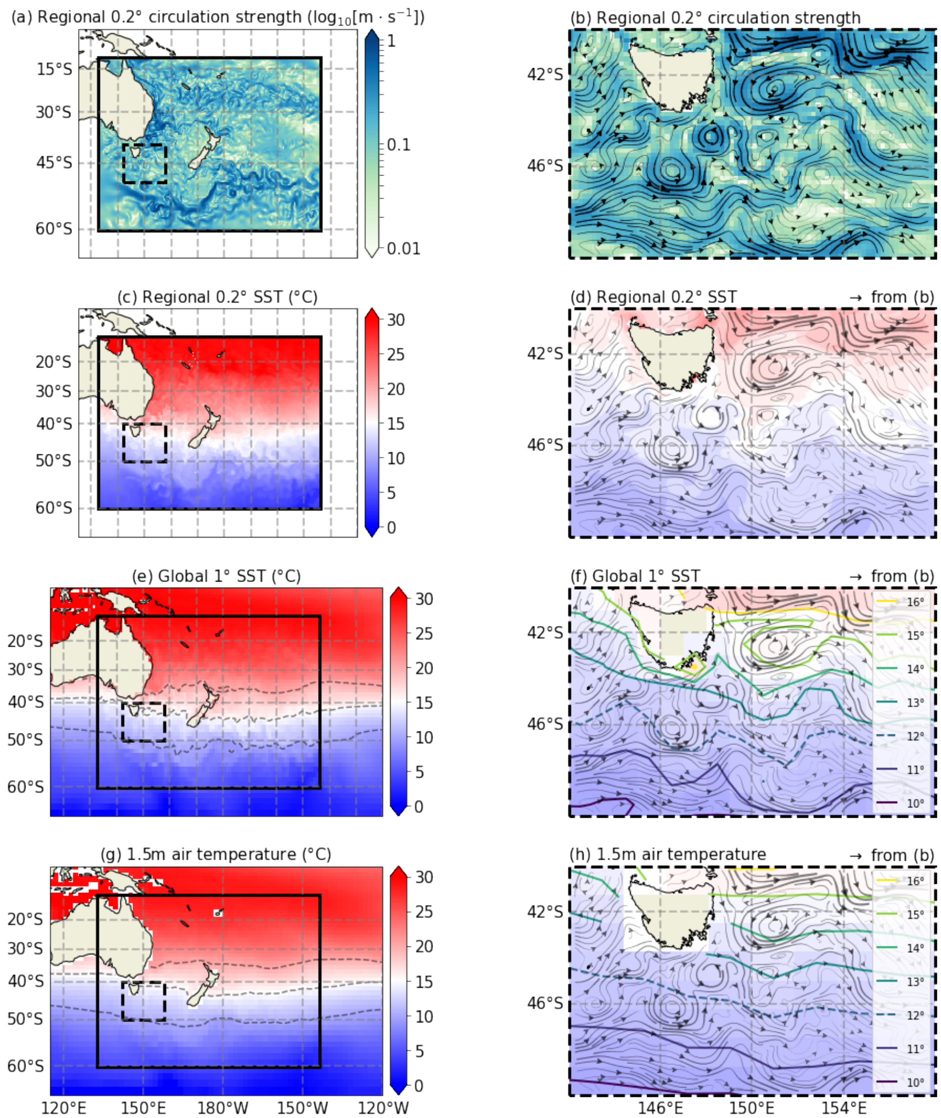

Figure 1: (a) Surface ocean circulation speed of the 0.2° nested ocean model. (b) As for (a) but zoomed into the dashed area and including vector streamlines with widths proportional to speed. (c) Sea surface temperature of the nested 0.2° ocean model. (d) As for (c) but zoomed into the dashed area and including the streamlines from (b). (e) Sea surface temperature from the 1° global ocean model. The 10, 15 and 20° isotherms are included to illustrate the increase in spatial 'noisiness' in the nested ocean region. (f) As for (e) but zoomed into the dashed area and including the streamlines from (b). Contours are at the same levels as the background colours and are intervals of 1°C from 10°C to 16°C and are described by the legend. The 10, 15 and 20° isotherms are included again to assist comparison with (e). (g) 1.5m air temperature at 1.25°×1.875°. The 10, 15 and 20°C isotherms are included as in (e). (h) As for (g) but zoomed into the dashed area and including the streamlines from (b). All sub-Figures on the same horizontal level – (a-b), (c-d) – have the same colour limits as indicated by the appropriate colour bar. All data is for the mean of January 1989.

[3] showed that sea surface temperatures - SSTs - in the region surrounding New Zealand are improved with respect to observations because of the better representation of ocean currents which the finer ocean grid allows. In particular, the transportation of heat and water volumes in the vicinity of the Tasman Front and the East Australian Current are improved which in turn improve the SST; indeed as [3] state:

'...the air-sea fluxes of heat and moisture over the [Tasman Sea] can be considered a pacemaker for New Zealand's weather and climate'.

Since this work and that of [3] use multi-decadal means, this improvement to the SSTs in the absence of any changes to the atmospheric physics means that 1.5m air temperature comes into equilibrium with the sea surface and improves its agreement with reanalysis data (see Figure 2).

Even at a resolution of 0.2° the nested region resolution is still not high enough for the model to be considered 'eddy resolving', however it *is* high enough to be 'eddy permitting'. This distinction is described in detail in e.g. [35]. Although the nested high-resolution ocean model is only run around New Zealand, the coarser global-ocean model is also run globally, including the AGRIF region. It is this lower-resolution model which is coupled to the atmosphere, and hence the detailed eddy-resolving structure of the underlying high-resolution ocean model is not passed to the atmosphere directly, but via a lower resolution intermediary. Work is underway to enable the atmosphere-ocean coupling to take place at higher resolution but this is not thought likely to substantially change the results presented here.

Figure 1 illustrates how the eddy activity in the nested ocean model is related to the air temperature. Figure 1(a) and (b) show the nested ocean's surface circulation speed at different length scales; the entire high-resolution region, and zoomed in to a particularly active eddy region south and west of Tasmania. (b) also shows circulation streamlines and these are also included in (d, f, h) to aid interpretation. The 2nd row – (c), (d) – show the sea surface temperature for the nested model. The 3rd row shows the SST in the same region but for the global, 1°, ocean model. (f) shows the zoomed in colours from (e) as well as contour levels at integer temperature values. Finally, the 4th row shows analogous sub-Figures as for the 3rd but for atmospheric temperatures.

There are two resolution mismatches to be considered here: (1) 0.2° nested ocean to 1° global ocean to; (2) 1° global ocean to 1.25°×1.875° atmosphere. The coupling between the ocean models is two-way but spatial information will naturally be lost in the upscaling procedure. That said, the evidence of the 'fingerprint' of the nested ocean on the global ocean model is clearly visible by comparing the SST field in Figure 1(e) inside and outside the nested region. This is even visible in the 1.5m air temperature – 1(g) – particularly around the northern reaches of the Antarctic Circumpolar Current at approximately 50°S and in the southward depression of the isotherms around 151°E in (h).

2.3 Validation datasets and metrics

We compare 20-year annual and seasonal means (1989-2008) of climate model output to observational and reanalysis products of temperature, total cloud amount, stratocumulus amount, and shortwave cloud radiative effect (SWCRE). The models runs are started in 1950 to enable model spin-up to occur and both models start from initial conditions from a UK Met Office simulations [36], which was itself run from 1850.

The simulated 1.5m temperatures, precipitation amounts and winds are compared to equivalent fields from the state-of-the-art ERA5 reanalysis [37]. Surface heat flux ground truth data are from the Objectively Analyzed Air–Sea Heat Fluxes dataset - hereafter 'OA flux' - of [38]. Cloud cover data is from the International Satellite Cloud Climatology project, ISCCP [39, 40].

2.4 NZESM runtime configuration

Given the significant computational expense of Earth System Models, it is very important to optimise the build and runtime configuration of the component model executables to achieve best efficiency. Ideal setups depend on the characteristics of the target high-performance computing (HPC) platform, such as the number of CPU cores per node, CPU architecture, choice of compilers and libraries, as well as the interconnect that is used for communicating data between the processes that run the model in parallel, and the storage system.

NZESM consists of separate executables for the atmosphere (Unified Model) and ocean (NEMO) components, which are coupled using the OASIS library. CPU cores on the HPC need to be distributed between these components to match their respective runtime between data exchanges as closely as possible, as any wait times will reduce efficiency. With the atmosphere model requiring many more cores than the ocean model to handle its much larger computational expense, just enough resources should be assigned to the ocean so that the atmosphere does not need to wait for data to arrive. OASIS comes with a timing feature to help find the right balance.

The Unified Model and NEMO use the Message Passing Library (MPI) for distributed parallel computing, where finding an optimal CPU core count for a given science configuration typically involves trade-offs between runtime and computational efficiency ("strong scaling"). While assigning more cores will speed up computation and thus achieve a higher number of model years per wall clock time interval, communication overheads become more and more important with increasing core count and reduce computational efficiency, as relatively more time needs to be spent on non-science related computation. It is usually advisable to start with a miminum number of cores that allows the model to meet runtime expectations at reasonable efficiency, especially on a busy HPC, where smaller core counts can lead to shorter queuing times and thus higher overall throughput. If communication overhead is still small and if there is enough capacity on the HPC, core counts can be increased to reduce runtime without suffering much efficiency loss ("linear scaling").

Both the Unified Model and NEMO impose constraints on how CPU cores can be used for parallel computing with the "domain decomposition" approach, which can prevent configurations from using all available cores on the assigned HPC nodes and thus impact efficient resource utilisation.

The Māui HPC that was used for this work comes with 40 Intel Skylake CPU cores per node. The original core count configuration of NZESM was readjusted for Māui to minimise atmosphere/ocean runtime imbalance, minimise the number of unused cores on the nodes, and maximise MPI parallelisation efficiency. This led to a 28% node count reduction from 32 nodes to 23 with only a modest 5% increase in runtime from 7.7 hours per model year to 8.1 hours per model year. Overall computational resource utilisation by NZESM was thus reduced by 24%.

3 Results

In the following sections we will explore the effect on the local atmospheric climate to the change in the ocean physics described above. We focus on changes to:

- Temperature at 1.5m and aloft.
- Tropopause height.
- Precipitation and evaporation.
- Surface latent and sensible heat fluxes.
- Zonal and meridional mean winds and the position of the sub-tropical jet stream.
- Occurrence of anticyclones in the storm track at New Zealand latitudes.
- Total cloud amount and its partitioning into morphological types.

3.1 Temperature

3.1.1 1.5m temperature

Figure 2 shows annual mean 1.5m air temperature for the UKESM and NZESM compared to ERA5 reanalysis data [37] for the period 1989-2008. The region defined by the blue rectangle in 2 denotes the location of the high-resolution nested ocean model. From here we refer to this as the AGRIF region, named after the method used to implement this change [3, 41, 34]. We can compare the atmosphere data shown in Figure 2 with equivalent

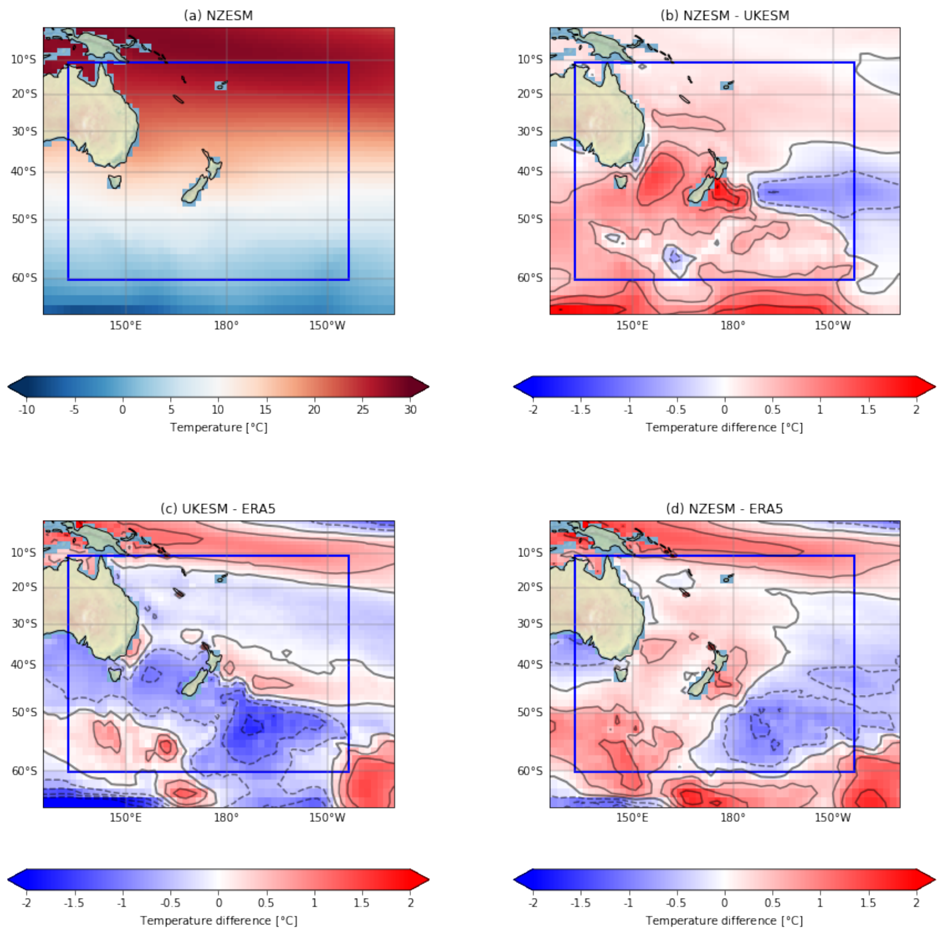

Figure 2: 1.5m annual mean air temperature (°C) for: (a) NZESM (b) NZESM - UKESM; (c) NZESM - ERA5 reanalysis; (d) UKESM - ERA5 reanalysis. All data shows annual means for 1989-2008.

ocean data in [3]. Figure 2(b) is analogous to the surface biases shown in Figure 9(a) in [3] and Figures 2(c-d) are analogous to Figures 8(a-b) in [3], although it should be noted that the latter case shows averages of the top levels of the ocean model down to 500m depth.

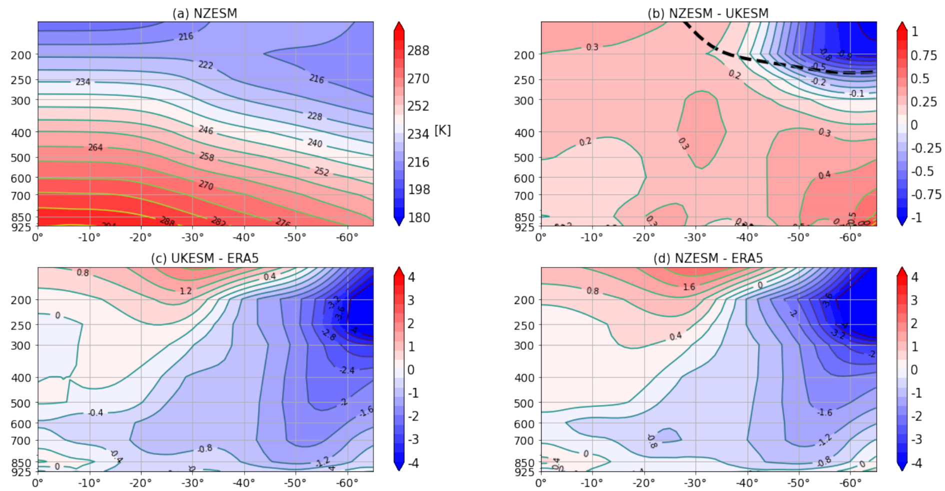

Figure 3: Temperature as a function of pressure: (a) NZESM, (b) NZESM - UKESM, and the NZESM tropopause in this region (c) NZESM - ERA5 reanalysis, (d) UKESM - ERA5 reanalysis. All data is for 1989-2008.

As noted above in section 2.2 there is less spatial variability - i.e. it is more homogeneous - in the atmosphere temperature field than in the equivalent ocean field in [3]. This is because of the lower resolution of the atmosphere model compared to the high-resolution nested ocean model.

The ocean data in [3] uses the EN4 climatology [42] for sea surface temperature and therefore this serves as a useful counterpoint to previous analyses with a different 'ground truth' dataset. Overall, the agreement with the ERA5 reanalysis is better in the NZESM compared to the UKESM, particularly in the vicinity of the AGRIF region although it should be noted that this is not the case universally.

The general warming seen at higher southern Latitudes in Figure 2 is also observed in the wider southern ocean region (not shown). This improvement-deterioration pair is often encountered in climate model development but it should be noted that we are presenting the behaviour as observed when the global ocean model physics is changed, rather than presenting the results of a tuning exercise. The tuning of climate models indeed has its own literature and the interested reader is referred elsewhere [43, 44, 45].

3.1.2 Temperature as a function of pressure

Figure 3 shows zonal mean temperature profiles for the entire region shown in Figure 2.

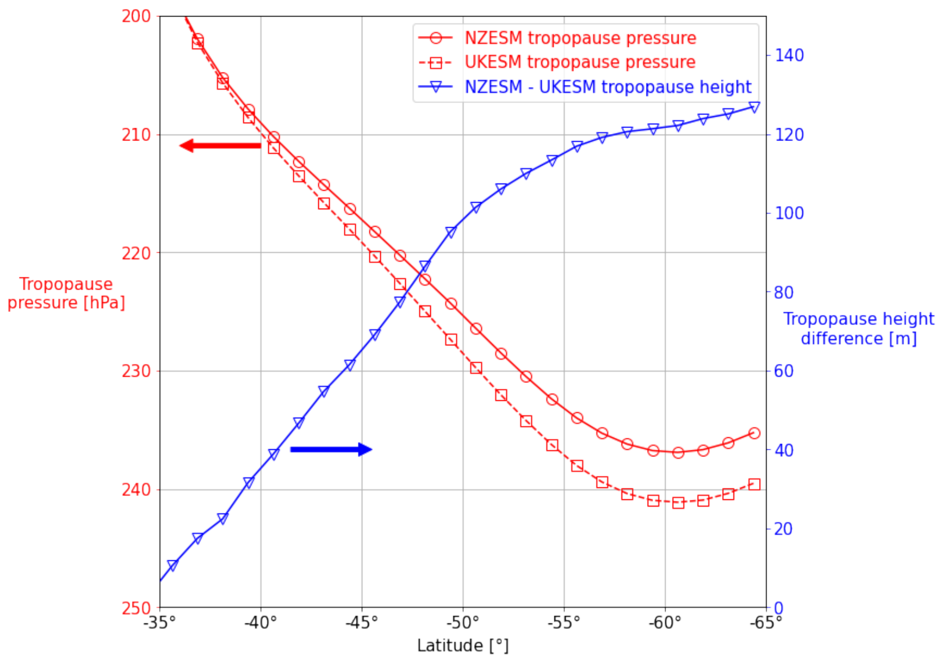

Figure 4: Tropopause pressures in Figure 3 (red) and the tropopause height *difference* (blue).

The tropospheric warming signal in the NZESM is clearly visible in Figure 3(b), as is the accompanying stratospheric cooling, which is expected to achieve overall energy balance [46].

The agreement between the tropospheric temperatures in the NZESM versus the reanalysis data is markedly improved compared to the UKESM in the mid-to-lower troposphere. There is some deterioration in the agreement in the stratosphere but this is of much smaller extent that the formerly mentioned improvement.

Figure 4 shows the tropospheric pressures for the models and the difference between the tropospheric heights. Due to the warming in the NZESM, the tropopause is raised by up to ≈130m. This is only ∼ 1% of the total height of the tropopause in this region, for comparison however, [47] shows that the global warming signal for 20°N – 80°N has been ≈ 50 - 60m per decade for the period 1980-2020.

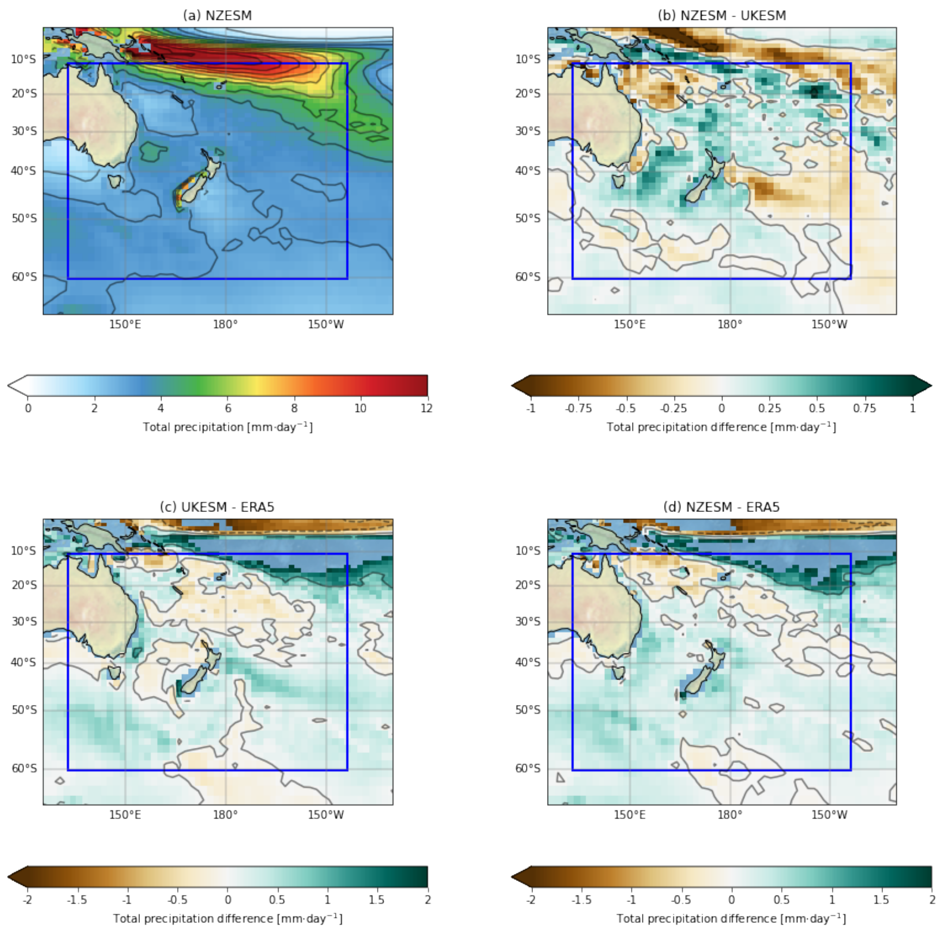

Figure 5: Total precipitation (mm · day^{-1}) for (a) NZESM, (b) NZESM - UKESM, (c) UKESM - ERA5, (d) NZESM - ERA5. Contour levels for levels for all plots are at integer values and for (c) and (d) values over 2mm · day^{-1} are masked to aid visual interpretation.

★

3.2 Precipitation minus evaporation

Figure 5 shows the annual mean total precipitation fluxes for the models against ERA5 reanalysis data.

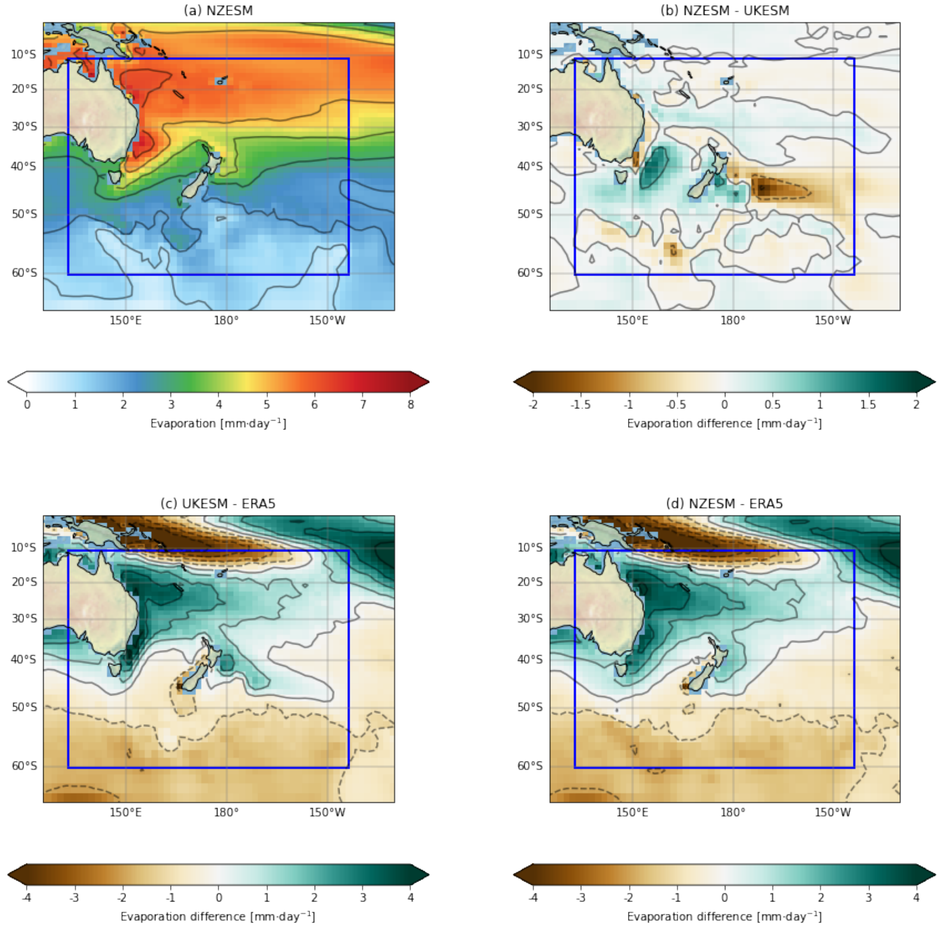

Figure 6: Sea to air evaporation (mm · day^{-1}) for (a) NZESM, (b) NZESM - UKESM, (c) UKESM - ERA5, (d) NZESM - ERA5. Contour levels for levels for all plots are at integer values.

From Figure 5(a) it is clear that by the largest contributor to the total precipitation in this region comes from the South Pacific Convergence Zone – SPCZ – in the northern portion of the Figure 5(a). This region of intense precipitation inclines south and eastwards from the Maritime Continent and shows a southward trend in the NZESM compared to the UKESM. This is evidenced by drying in the northern portion and the opposite in the southern portion in the northeast of Figure 5(b). This sub-figure also shows a general drying to the east and a moistening to the west of New Zealand, which is anti-correlated to the 1.5m temperature changes observed in Figure 2(b).

Comparing Figures 5(c) and (d) we see that the NZESM reduces both wet and dry biases close to New Zealand and that the southward shifting of the SPCZ is evident in the more concentrated drying signal in Figure 5(d) with respect to ERA5.

Figures 6 and 7 show sea to air evaporation flux and precipitation minus evaporation ($P - E$) for the models and ERA5 respectively.

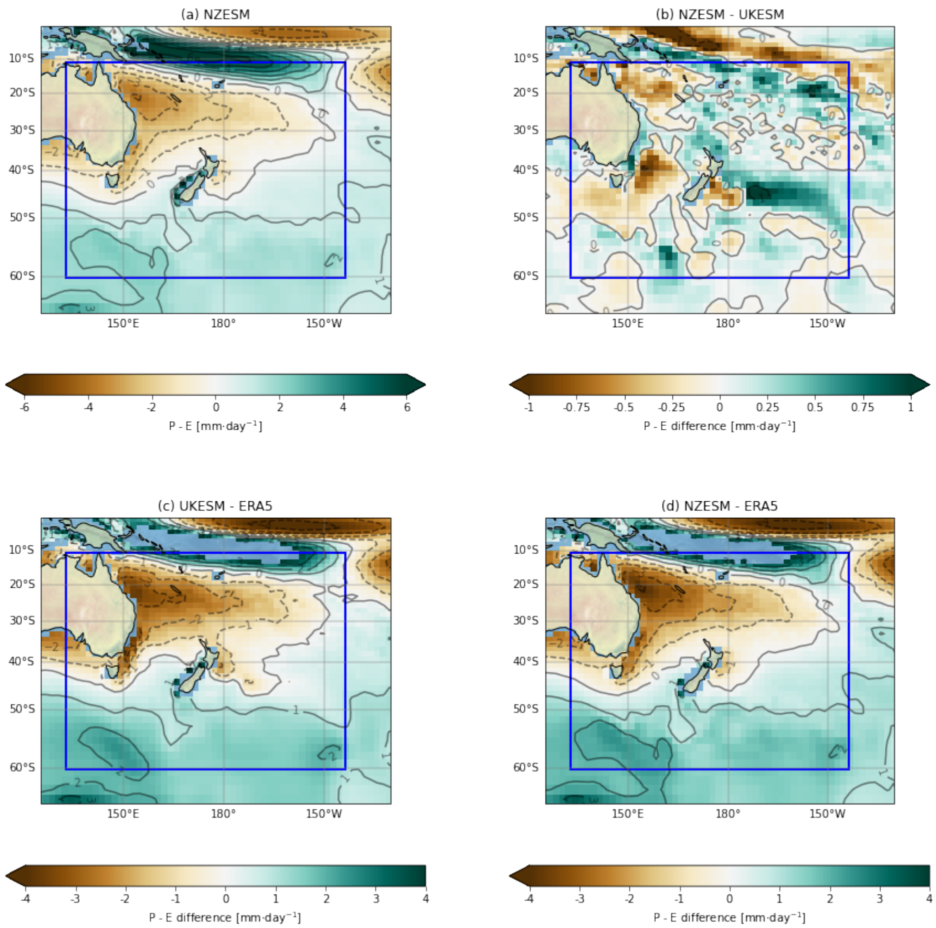

Figure 7: $P - E$ ($\mathrm{mm} \cdot \mathrm{day}^{-1}$) for (a) NZESM, (b) NZESM - UKESM, (c) UKESM - ERA5, (d) NZESM - ERA5. Contour levels for levels for all plots are at integer values and for (c) and (d) values over $4\mathrm{mm} \cdot \mathrm{day}^{-1}$ are masked to aid visual interpretation.

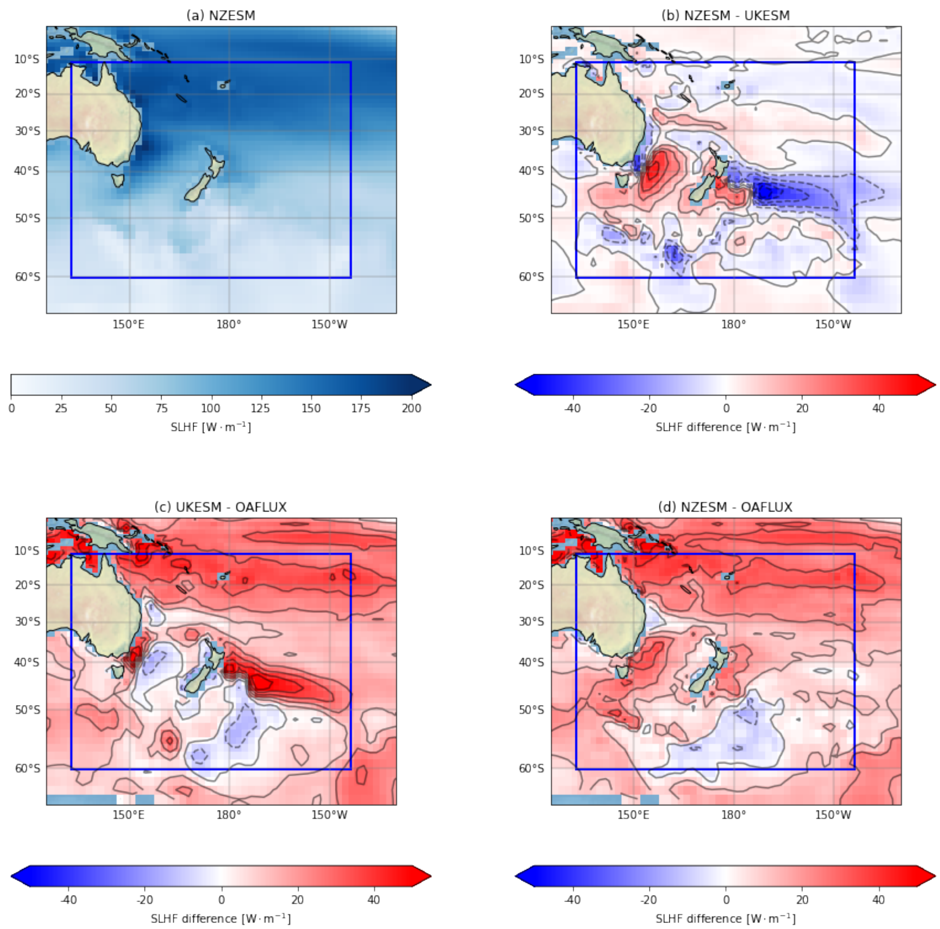

Figure 8: Surface latent heat fluxes ($W{\cdot}m^{-2}$) for (a) NZESM (b) NZESM - UKESM; (c) NZESM - OA flux; (d) UKESM - OA flux.

Overall, the pattern of changes in the evaporation are of the same sign as the precipitation. That is, regions which show more precipitation also show more evaporation, and vice versa. However, the changes to the evaporation flux are generally larger than the changes to precipitation and hence the region to the east of New Zealand shows positive $P - E$ change even though the amount of precipitation in this region is decreased. The sign of this effect is reversed over the Tasman Sea which shows an overall 'drying' – negative $\Delta(P - E)$ – in spite of increasing precipitation.

3.3 Surface heat balance

As discussed above, the Southern Ocean region has well-known and longstanding model biases in climate model simulations. In this section we explore the effect of the eddy-permitting ocean on latent and sensible heat balances at the surface.

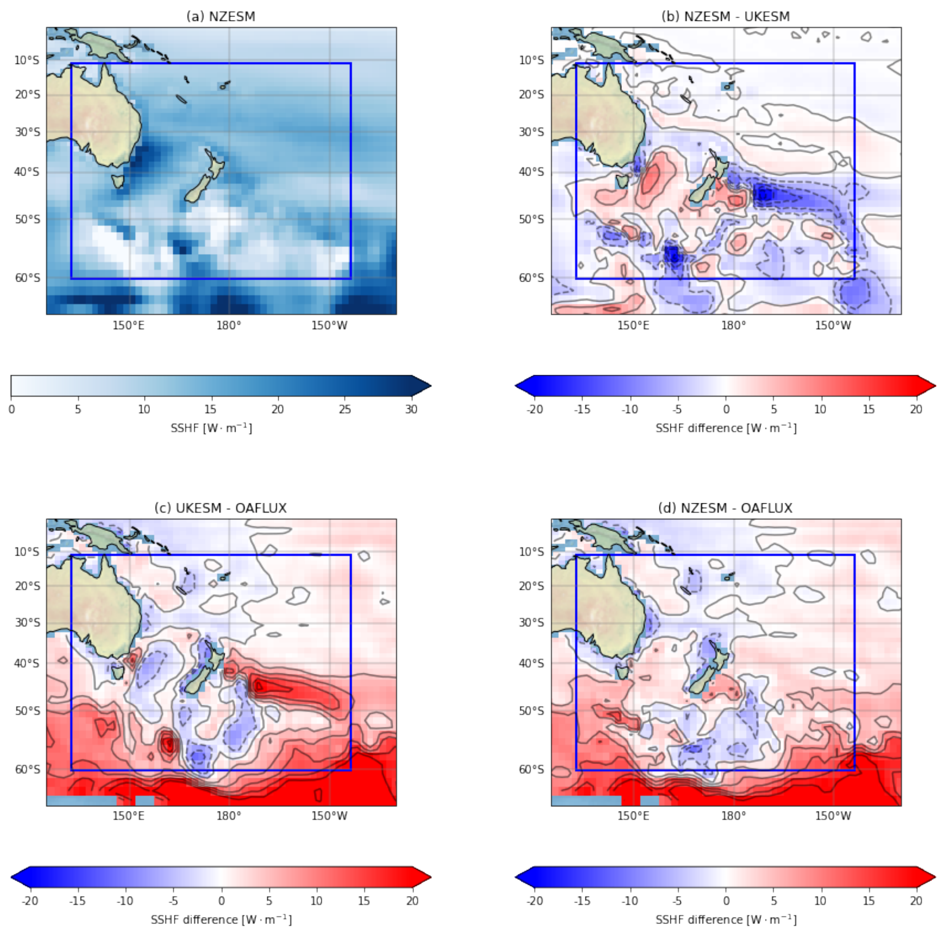

Figure 9: Surface sensible heat fluxes (W·m^{-2}) for (a) NZESM (b) NZESM - UKESM; (c) NZESM - OA flux; (d) UKESM - OA flux.

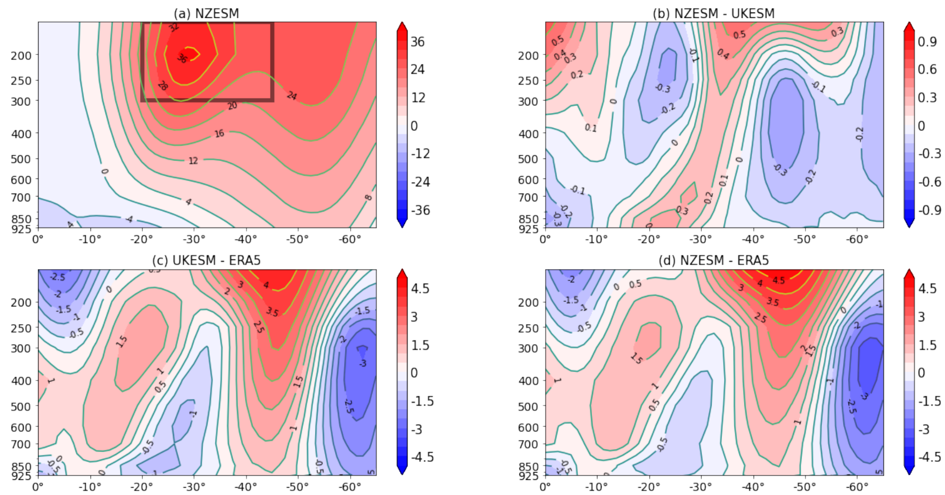

Figure 10: Zonal mean zonal wind ($m \cdot s^{-1}$) for: (a) NZESM (b) NZESM - UKESM; (c) NZESM - ERA5 reanalysis; (d) UKESM - ERA5 reanalysis. The box in (a) shows the area which is region which is examined in more detail in Figure 11.

Figures 8 and 9 show the surface latent and sensible heat fluxes respectively for the models versus the OA flux dataset [38].

The overall structure of these two figures is - as expected - very similar to temperature response in Figure 2. In both cases, the model-data agreement is improved in the NZESM and this is particularly striking in the case of the sensible heating, which shows – for example – significantly improved model-reanalysis agreement to the east of New Zealand.

In the case of the latent heating there are some areas of improvement (region of convergence of the Southland and East Auckland Currents) and deterioration (Tasman Sea and the south east coast of Australia in particular). That said, there is a clear overall improvement in the model-data agreement in Figure 8.

3.4 Winds

3.4.1 Zonal mean zonal wind

New Zealand's climate is primarily maritime-driven and the prevailing westerly winds are a key driver of – for example – (South Island) West Coast extreme rainfall [48]. Firstly we study the east-west component of the wind, *u*, defined positive west to east. Figure 10 shows the zonal mean zonal wind for the region shown in the maps in previous figures.

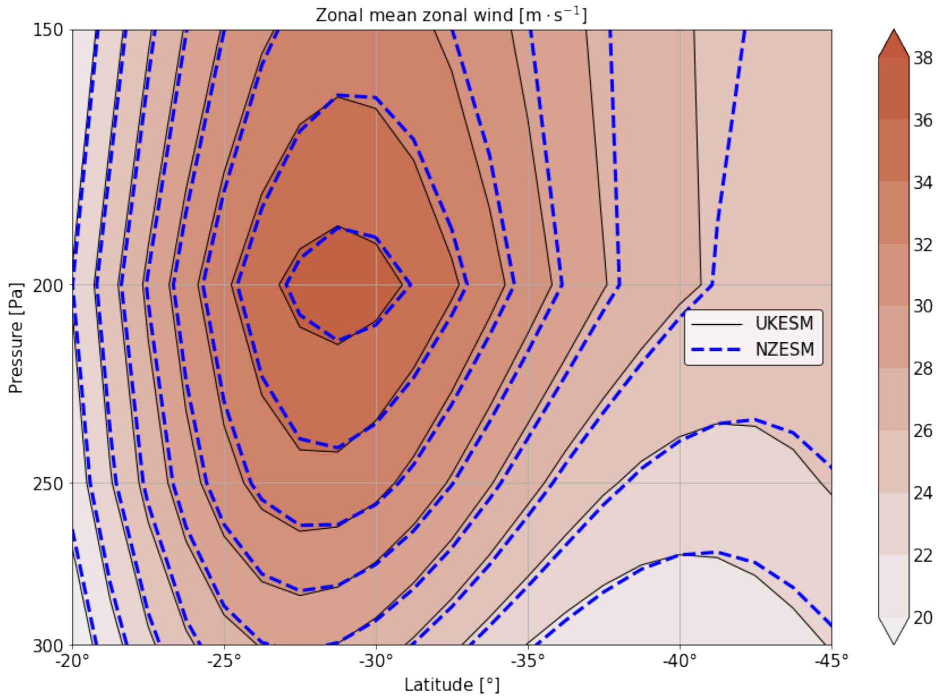

Figure 11: Zonal means zonal wind (m · s^{-1}) in the region bounded by the black box in Figure 10(a).

In Figure 10(a) the dominance of the westerlies is clearly visible in the mostly-positive sign of u. The subtropical jet is clearly visible at around 200hPa and ≈ 30°S. This is shown by the black box in Figure 10(a) and examined in more detail in Figure 11. Figure 10(b) shows that there is a small but non-negligible southward shift of the jet in the NZESM and (c), (d) show a general improvement in model-reanalysis agreement, particularly at latitudes north of ≈ -30°S .

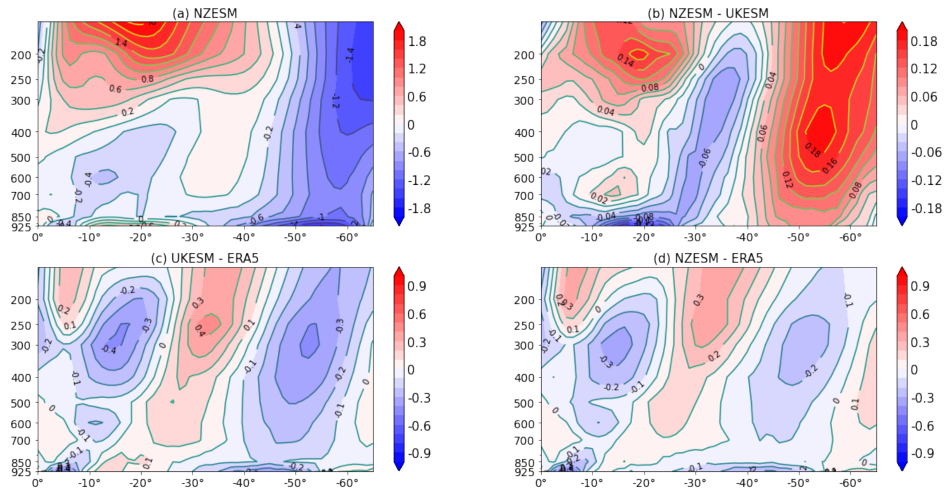

Figure 12: Zonal mean meridional wind ($m \cdot s^{-1}$) for (a) NZESM (b) NZESM - UKESM; (c) NZESM - ERA5 reanalysis; (d) UKESM - ERA5 reanalysis.

Figure 11 shows a close-up of the region indicated by the box in Figure 10(a) and shows a southward shift of the sub-tropical jet which increases with decreasing latitude. Indeed, in some areas, the southward shift is as much as $1°$, or ≈100km.

This small but non-negligible change to the position of the jet is indicative of a general southward shift in the westerlies. The effect of this on the storm track impinging on New Zealand is discussed in §3.5.

3.4.2 Zonal mean meridional wind

Figure 12 shows the equivalent figure to Figure 10 but for the meridional wind, v, conventionally positive south to north. The improvement to the structure of v as a function of pressure is striking, with the magnitude of both positive and negative biases reduced almost universally. Additionally, the fractional change to v in Figure 12 is in fact significantly greater than the changes to u in Figure 10.

This improvement is likely attributable to the significant improvement in the latitudinal structure of the near-surface temperature, see Figures 3(c),(d)

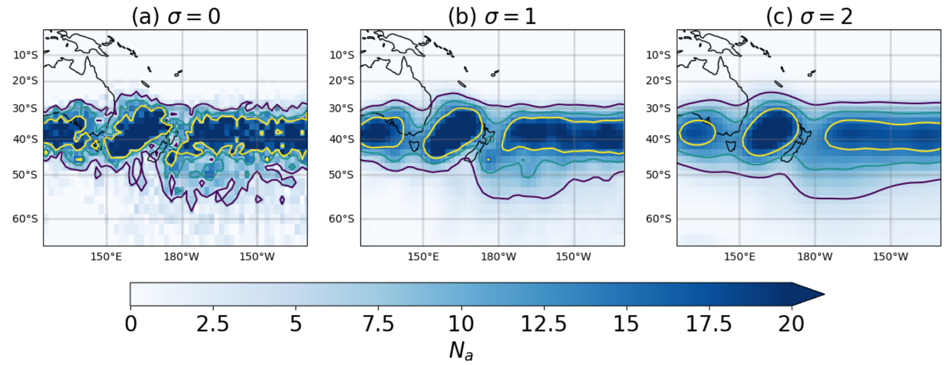

Figure 13: Storm tracks, i.e. the number of unique anticyclonic storms - N_a - for the NZESM. The σ value is the Gaussian kernel standard deviation used by the `SciPy` software [50].

3.5 Storm track

In this section we use the `stormTracking` package (https://github.com/ecjoliver/stormTracking) to generate maps of the number of unique anticyclones - N_a - in 6-hourly mean sea level pressure data. This software uses the mesoscale feature tracking capability described in [49].

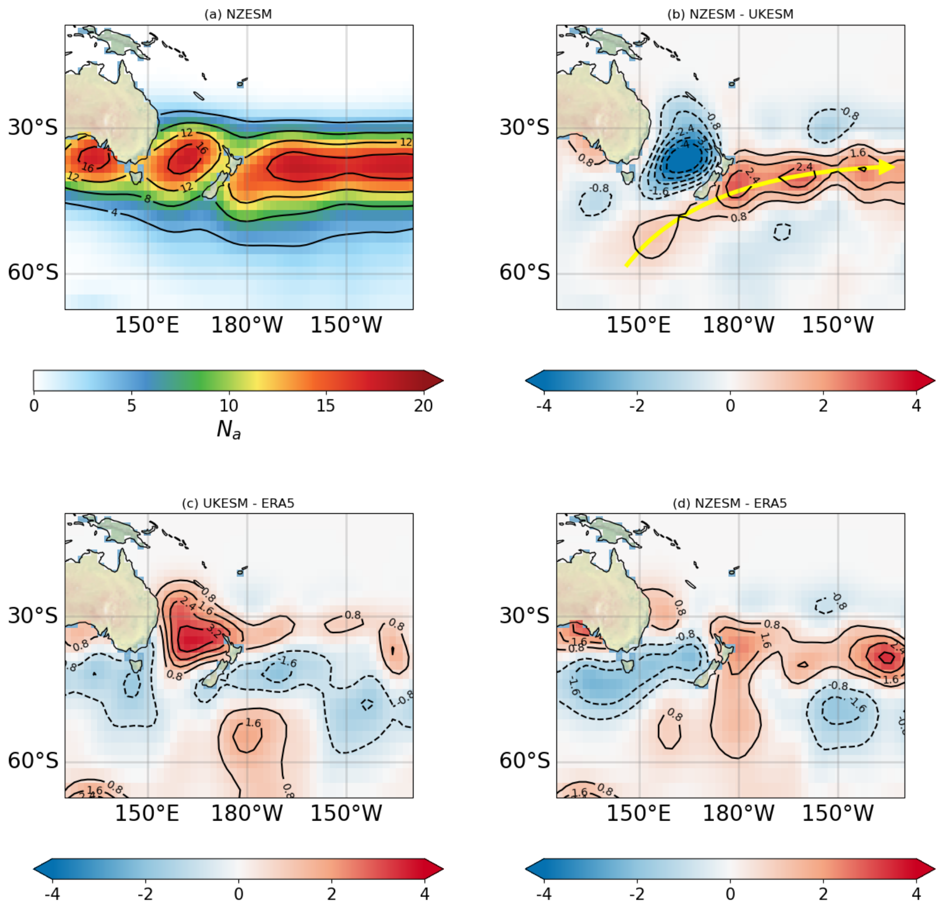

Figure 14: N_a for (a) NZESM – as in Figure 13(c) – (b) NZESM - UKESM with yellow arrow indicating the alteration of the storm track; (c) NZESM - ERA5 reanalysis; (d) UKESM - ERA5 reanalysis using $\sigma = 2$ in the Gaussian smoothing calculations.

Figure 13(a) shows raw N_a data for ERA5 and sub-figures (b) and (c) show the same data but with a Gaussian smoothing applied with standard deviations - σ - of 1 and 2 respectively. The function used is the `gaussian_filter` function in the multidimensional image processing package of `SciPy` [50] (version `1.8.0`). This smoothing is performed to assist in interpreting the differences between the ERA5 data and the model simulations due to the spatial noise in the unsmoothed data, i.e. Figure 13(a). The N_a maps are shown in Figure 14 and the zonal structure of the storm track is immediately clear.

Figure 14 shows that the storm track in shifted south in the NZESM – yellow arrow in Figure 14(b) – and that there is a significant reduction in the number of storms over the Tasman Sea. This reduction leads to a noticeably better agreement between the NZESM and ERA5 in this region. A more detailed exploration of the models' storm climatologies and how they are predicted to change over the course of the 21st century is the subject of ongoing research and will be published elsewhere.

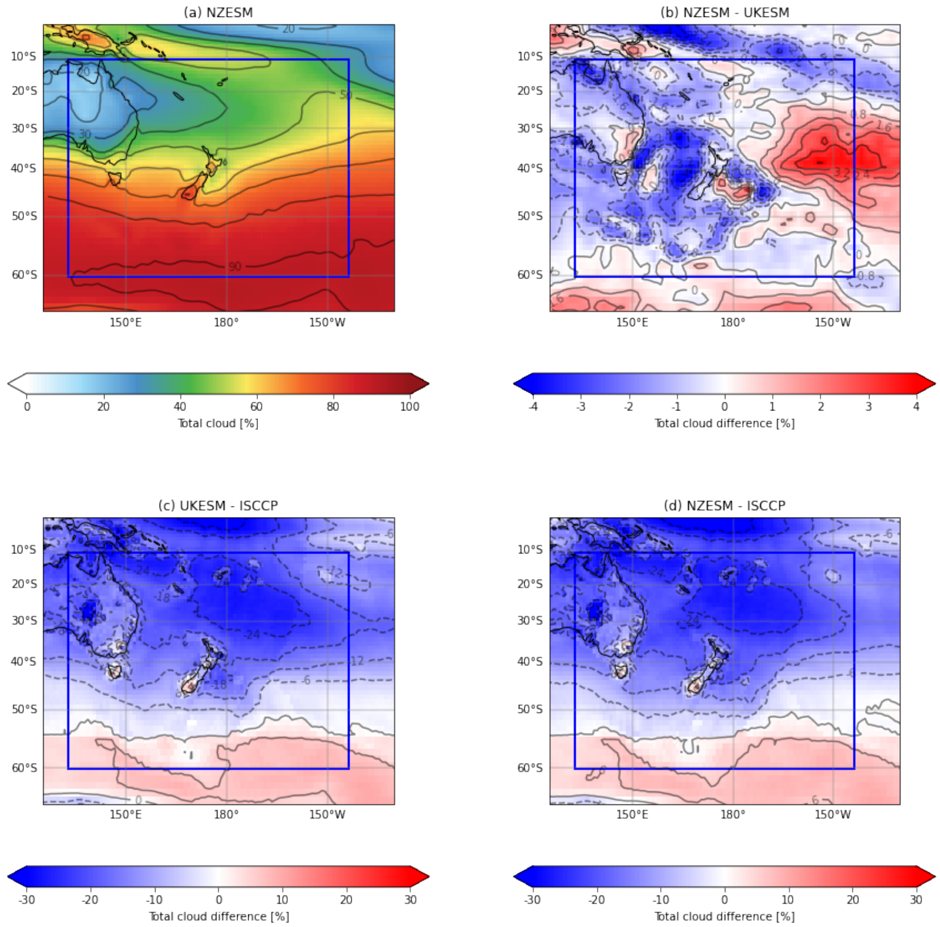

Figure 15: Total cloud for (a) ISCCP observations, (b) NZESM - UKESM, (c) UKESM - ISCCP, (d) NZESM - ISCCP.

3.6 Clouds

Figure 15 shows the total cloud amount from the models and observations from the International Satellite Cloud Climatology Project, ISCCP [39].

Cloud type	Morphological type	CTP [hPa]	Optical depth, τ
High top thin	Cirrus	P < 440	$0.3 < \tau < 3.6$
High top medium	Cirrostratus	P < 440	$3.6 < \tau < 23$
High top thick	Deep Convection	P < 440	$23 < \tau$
Mid-level top thin	Altocumulus	440 < P < 680	$0.3 < \tau < 3.6$
Mid-level top medium	Altostratus	440 < P < 680	$3.6 < \tau < 23$
Mid-level top thick	Nimbostratus	440 < P < 680	$23 < \tau$
Low top thin	Cumulus	P > 680	$0.3 < \tau < 3.6$
Low top medium	Stratocumulus	P > 680	$3.6 < \tau < 23$
Low top thick	Stratus	P > 680	$23 < \tau$

Table 1: Representative morphological cloud types from [52].

Figure 15(b) shows that there is a general increase in cloud to the east of New Zealand with the reverse seen to the west and south in the Tasman Sea, and in the SPCZ. At mid-latitudes, the sign of this change is anti-correlated with the temperature change and in the SPCZ there is a clear relationship between the reduction in total cloud and the amount of precipitation, Figure 5(b). These intra-model differences notwithstanding, it should be noted that the differences between the models and the observations are order of magnitude larger.

The response of clouds to climate perturbations is one of the most uncertain aspects of climate change and although it is useful to examine the total cloud amount, it is instructive to split the total into into constituent morphological types. A commonly used technique in climate model validation – e.g. [51] – is to partition the clouds into 9 categories or 'bins' of cloud-top-height and optical depth. These 9 categories correspond approximately to the 9 morphological types in Table 1 [52].

The 9 types in Table 1 are themselves combinations of a larger set of 7 cloud-top-pressure and 7 optical depth, τ, bins which are defined by the Cloud Feedback Model Intercomparison Project Observational Simulator Package, COSP Figure 2(c) in [51] and Figure 16(a). This package processes model outputs so that they can be compared directly with satellite retrievals. Note the 'zeroth' category in Figure 16(a) which contains clouds which are too optically thin to be detected by the satellites. Figure 16(b) shows the 9 cloud types in the ISCCP for 1989-2008.

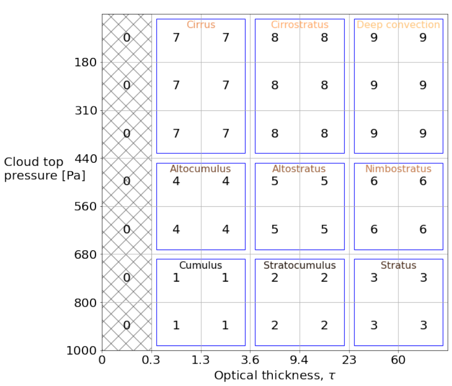

(a) Cloud top pressure versus optical depth, τ. This shows the categorisation of the 7×7 ISCCP data into the 3×3 matrix used for model-data comparison. This data is shown numerically in Table 1

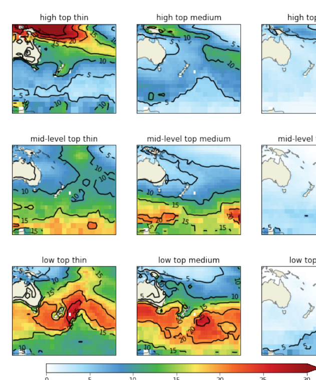

(b) Annual mean CTP-τ histograms for the ISCCP dataset, 1989 - 2008.

Figure 16

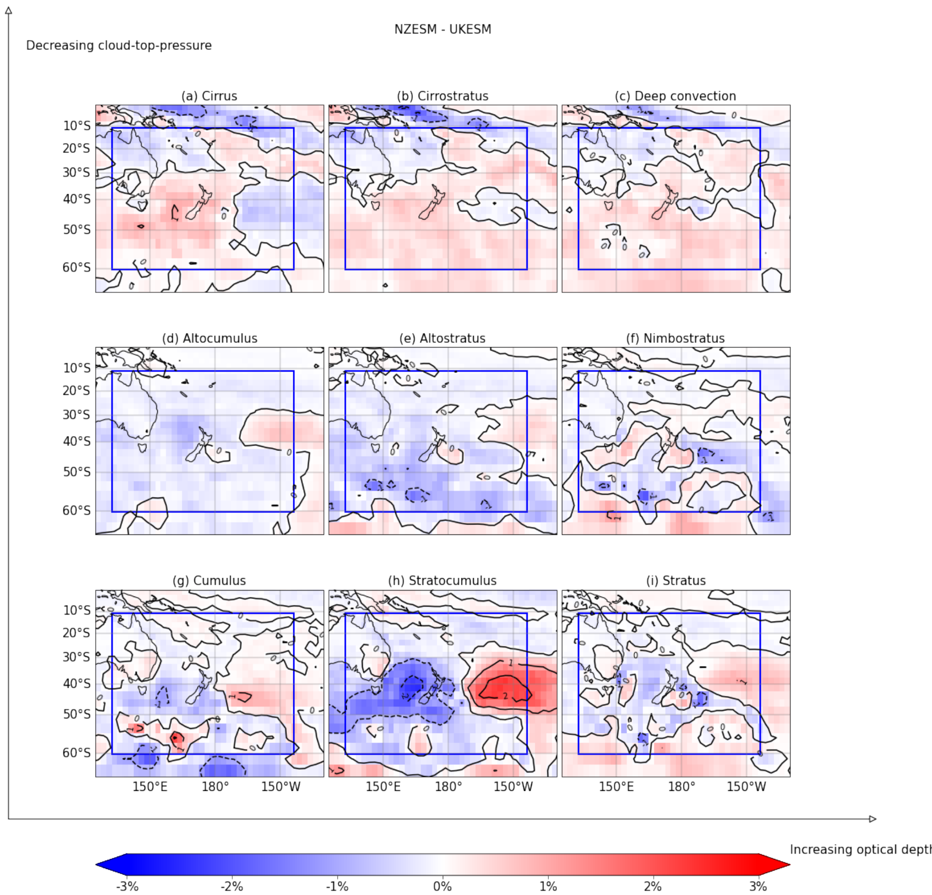

Figure 17: NZESM - UKESM cloud type occurrence differences.

For the models, the differences between the cloud types are shown in Figure 17. Figure 17 shows firstly that the magnitude of the cloud occurrence differences are small compared to the observed amounts in Figure 16(b) and also that the only morphological type which differs substantially between the models is stratocumulus (Sc), Figure 17(h).

There is a clear anti-correlation between stratocumulus amount in Figure 17(h) and 1.5m temperature differences in Figure 2(b) between ≈ -50 to -30°S. For Sc, the magnitude of this change is $\sim 1\% \cdot \mathrm{K}^{-1}$, which is in good agreement with the data from Figure 5 in [53] for a similar cloud type categorisation type. It should be noted in Figure 17(h) however that at higher southern latitudes, the sign of the correlation is reversed. This corresponds closely to the location of the austral winter sea ice maximum. Indeed, for the austral summer (DJF), the anti-correlation between temperature and Sc is dominant across the domain, but for austral winter (JJA), this reversed around the sea ice edge, in agreement with, for example, [54] Table 1, which shows a negative correlation between sea ice area and cloud fraction south of $\approx -55°$.

To quantify this further, for each latitude, λ, we have calculated the the correlation coefficient, c_λ, between the DJF and JJA temperature differences, ΔT_λ, and the equivalent stratocumulus amounts, ΔS_λ. The unnormalised, c_λ, and normalised, $c_{\lambda,N}$, quantities are plotted in Figure 18 and are defined in equations 1 and 2 respectively,

$$c_\lambda = \sum_\theta \left\{ \Delta T_{\lambda,\theta} \cdot \Delta S_{\lambda,\theta} \right\} \tag{1}$$

$$c_{\lambda,N} = \frac{c_\lambda}{\left| \Delta T_{\lambda,\theta} \cdot \Delta S_{\lambda,\theta} \right|_{\max}} \tag{2}$$

where θ represents the longitude values at each latitude, λ.

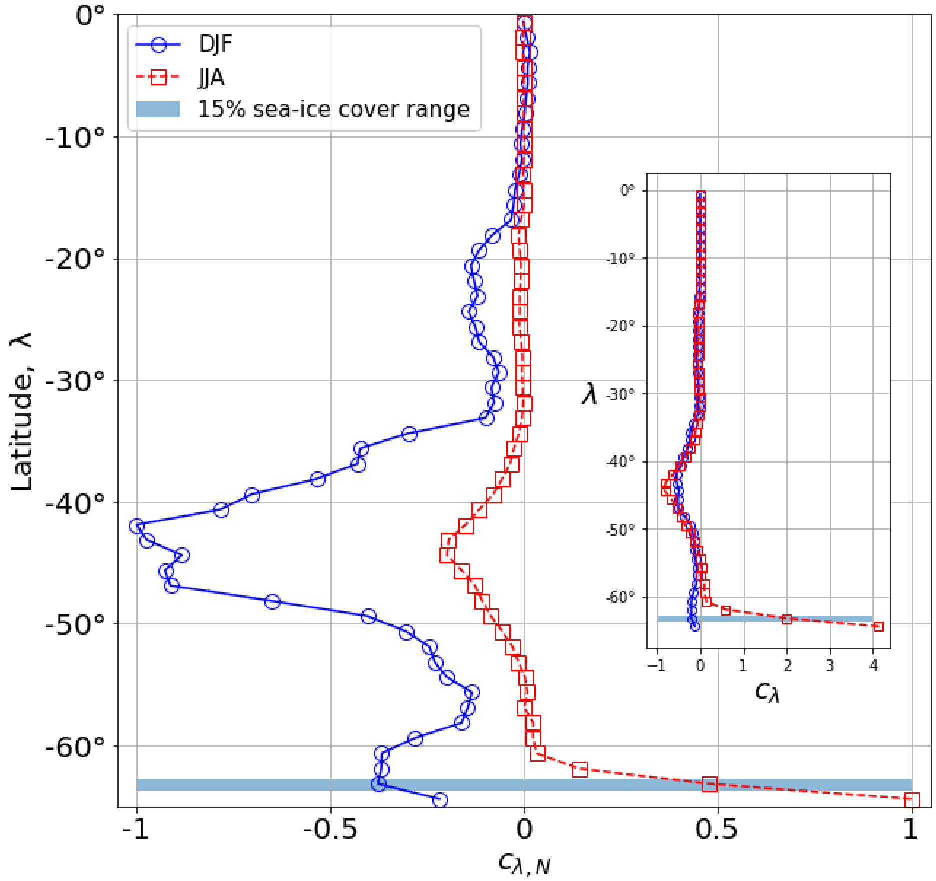

Figure 18: Normalised, c_λ and unnormalised, $c_{\lambda,N}$ – inset – correlation between temperature and stratocumulus amount differences (NZESM - UKESM) for austral winter, JJA, and summer, DJF, in the region shown in Figure 17. The shaded bar just south of -60° shows the difference between the latitudes of the 15% sea ice contour for the two models, with the NZESM being shifted ∼1°, or ≈100km southward.

Figure 18 shows that, in austral summer, the sign of the correlation between temperature and stratocumulus amount is almost universally negative, with the exception of some negligibly small positive values near the equator. In austral winter however, the sign of the correlation is reversed southward of approximately -60°S, which coincides with the location of the seasonal sea-ice edge. The blue shaded region south of -60°S in Figure 18 shows the average latitude of the 15% isopleth of JJA sea ice cover in the region considered, which is a commonly-used measure of sea ice extent [55]. Southward of the sea ice edge, the c_λ values become up to 4 times the magnitude of any negative values at latitudes nearer the equator. This indicates that the sea-ice retreat in the NZESM – ultimately due to increased heat transport south from the eddy-permitting ocean – has a significant effect on the resulting cloud amount and shows the efficacy of studying this inherently coupled ‘system of systems’ with a model of appropriate complexity [56].

4 Conclusions

In this work we have studied the regional atmospheric climate of two historical simulations of the period 1989 - 2008 using configurations of the UKESM1.0 model with [3] and without [33, 4] a nested, regional ocean model. The introduction of the eddy-permitting ocean model improves many aspects of model-observation agreement (underlined text for easy reference):

- The 1.5m air temperature closely mirrors the improvements seen in the equivalent plots shown in [3]. This is of course expected since the data presented are multi-decadal annual means for the same model pair. The atmosphere data however shows less spatial variability compared to the ocean and this is due to the lower atmospheric resolution and the fact that the coupling between the model components is performed at the global ocean model resolution.
- For the air temperature above the boundary layer, the NZESM exhibits tropospheric warming and stratospheric cooling, the former of which leads to a significant improvement in model-reanalysis agreement and a raising of the tropopause height by ≈130m, or ∼1%, which is comparable to the climate change signal in the same quantity over recent decades.
- The SPCZ dominates the precipitation signal in the region studied here and shows a southward shift in the NZESM *cf.* the UKESM. The NZESM also shows reduced wet *and* dry biases close to New Zealand.
- The changes to sea-to-air evaporation are generally of the same sign as the precipitation changes, but larger in magnitude meaning that $\Delta(P - E)$ is of the opposite sign to ΔP in some areas.
- The surface heat balance in the NZESM is improved with respect to observations. This is true for both the latent and sensible heat fluxes but is particularly striking for the latter. In common with virtually all model development changes – see below – the observed changes are not all beneficial. For example, the latent heat fluxes are improved in the convergence region of the Southland and East Auckland Currents but degraded over the Tasman sea. Overall however, the improvements are beneficial to model performance, even in the absence of additional model tuning.
- The zonal mean zonal wind, u, exhibits a southward shift of the sub-tropical jet by ≈100km and an overall improvement in model-reanalysis agreement, particularly at latitudes north of ≈ -30°S.
- The zonal mean meridional wind, v, in the NZESM shows almost universal improvements to the positive and negative biases in the UKESM. This is likely attributable to the overall improvement in the latitudinal structure of the air temperature aloft.
- Preliminary results on the effect of the high-resolution ocean model on the mid-latitude storm track shows two main features. Firstly, a significant reduction in the number of anticyclonic systems over the Tasman Sea and secondly a general southward shift of the storm track to the east of New Zealand.
- With respect to clouds, the first-order effect of the NZESM's high-resolution ocean is to increase total cloud cover to the east of New Zealand and to decrease it over the Tasman sea and the SPCZ. These cloud changes are generally anti-correlated with surface temperature changes at mid-latitudes but the reverse is seen further south. This change to a positive cloud-amount temperature correlation is attributed to the location of the seasonal sea-ice edge south of ≈ -60° S and its concomitant effect on stratocumulus cloud amount in particular.

In the NZESM there is some deterioration in the 'far field' sea surface temperature in the Southern ocean compared to observations; a region that already suffered from longstanding biases. Climate models are often tuned [43, 44, 45] to minimise and balance biases and therefore, making a major change to the regional ocean physics without further tuning, is likely to degrade model performance in some areas. Put another way, some of the bias that the tuning was compensating for is no longer there in the NZESM.

Future work using this nesting methodology on other similarly-related model pairs, as well as this same model pair in different regions of the Southern Ocean – and even elsewhere – would be of significant interest. Additionally, nesting of a high-resolution atmosphere within the global, coupled model would complement the longstanding history of regional atmosphere modelling in New Zealand, e.g. [57].

Acknowledgements

This paper obtained funding and support through the Ministry of Business Innovation and Employment Deep South National Science Challenge projects (C01X1412) and Royal Society Marsden Fund (NIW1701). The development of the UKESM, was supported by the Met Office Hadley Centre Climate Programme funded by BEIS and Defra (GA01101) and by the Natural Environment Research Council (NERC) national capability grant for the UK Earth System Modelling project, grant number NE/N017951/1. The authors would also like to acknowledge the support and collaboration of the wider Unified Model Partnership, https://www.metoffice.gov.uk/research/approach/collaboration/unified-model/partnership. and the use of New Zealand eScience Infrastructure (NeSI) high performance computing facilities, consulting support and training services as part of this research. New Zealand's national facilities are provided by NeSI and funded jointly by NeSI's collaborator institutions and through the Ministry of Business, Innovation & Employment's Research Infrastructure programme, www.nesi.org.nz. The ocean and sea-ice code used in this work is available online at https://doi.org/10.5281/zenodo.3873691.

References

[1] Veronika Eyring et al. "Overview of the Coupled Model Intercomparison Project Phase 6 (CMIP6) experimental design and organization". In: *Geoscientific Model Development* 9.5 (May 2016), pp. 1937–1958. DOI: 10.5194/gmd-9-1937-2016. URL: https://doi.org/10.5194%5C%2Fgmd-9-1937-2016.

[2] J. Williams et al. "Development of the New Zealand Earth System Model: NZESM". In: *Weather and Climate* 36 (2016), pp. 25–44. ISSN: 01115499. URL: https://www.jstor.org/stable/26779386 (visited on 02/07/2023).

[3] Erik Behrens et al. "Local Grid Refinement in New Zealand's Earth System Model: Tasman Sea Ocean Circulation Improvements and Super-Gyre Circulation Implications". In: *Journal of Advances in Modeling Earth Systems* 12.7 (2020). e2019MS001996 2019MS001996, e2019MS001996. DOI: https://doi.org/10.1029/2019MS001996. URL: https://agupubs.onlinelibrary.wiley.com/doi/abs/10.1029/2019MS001996.

[4] Alistair A. Sellar et al. "Implementation of U.K. Earth System Models for CMIP6". In: *Journal of Advances in Modeling Earth Systems* 12.4 (2020). e2019MS001946 10.1029/2019MS001946, e2019MS001946. DOI: https://doi.org/10.1029/2019MS001946. URL: https://agupubs.onlinelibrary.wiley.com/doi/abs/10.1029/2019MS001946.

[5] J.-B. Sallée et al. "Assessment of Southern Ocean water mass circulation and characteristics in CMIP5 models: Historical bias and forcing response". In: *Journal of Geophysical Research: Oceans* 118.4 (Apr. 2013), pp. 1830–1844. DOI: 10.1002/jgrc.20135. URL: https://doi.org/10.1002%5C%2Fjgrc.20135.

[6] Jennifer E. Kay et al. "Global Climate Impacts of Fixing the Southern Ocean Shortwave Radiation Bias in the Community Earth System Model (CESM)". In: *Journal of Climate* 29.12 (June 2016), pp. 4617–4636. DOI: 10.1175/jcli-d-15-0358.1. URL: https://doi.org/10.1175%2Fjcli-d-15-0358.1.

[7] A. Bodas-Salcedo et al. "Large Contribution of Supercooled Liquid Clouds to the Solar Radiation Budget of the Southern Ocean". In: *Journal of Climate* 29.11 (May 2016), pp. 4213–4228. DOI: 10.1175/jcli-d-15-0564.1. URL: https://doi.org/10.1175%5C%2Fjcli-d-15-0564.1.

[8] Patrick Hyder et al. "Critical Southern Ocean climate model biases traced to atmospheric model cloud errors". In: *Nature Communications* 9.1 (Sept. 2018). DOI: 10.1038/s41467-018-05634-2. URL: https://doi.org/10.1038%2Fs41467-018-05634-2.

[9] Vidya Varma et al. "Improving the Southern Ocean cloud albedo biases in a general circulation model". In: *Atmospheric Chemistry and Physics* 20.13 (July 2020), pp. 7741–7751. DOI: 10.5194/acp-20-7741-2020. URL: https://doi.org/10.5194%2Facp-20-7741-2020.

[10] A. Bodas-Salcedo et al. "The Surface Downwelling Solar Radiation Surplus over the Southern Ocean in the Met Office Model: The Role of Midlatitude Cyclone Clouds". In: *Journal of Climate* 25.21 (Nov. 2012), pp. 7467–7486. DOI: 10.1175/jcli-d-11-00702.1. URL: https://doi.org/10.1175%5C%2Fjcli-d-11-00702.1.

[11] A. Yool et al. "Evaluating the physical and biogeochemical state of the global ocean component of UKESM1 in CMIP6 historical simulations". In: *Geoscientific Model Development* 14.6 (2021), pp. 3437–3472. DOI: 10.5194/gmd-14-3437-2021. URL: https://gmd.copernicus.org/articles/14/3437/2021/.

[12] Matt Hawcroft et al. "Southern Ocean albedo, inter-hemispheric energy transports and the double ITCZ: global impacts of biases in a coupled model". In: *Climate Dynamics* 48.7-8 (June 2016), pp. 2279–2295. DOI: 10.1007/s00382-016-3205-5. URL: https://doi.org/10.1007%5C%2Fs00382-016-3205-5.

[13] Karl E Taylor, Ronald J Stouffer, and Gerald A Meehl. "An overview of CMIP5 and the experiment design". In: *Bulletin of the American meteorological Society* 93.4 (2012), pp. 485–498.

[14] Baijun Tian and Xinyu Dong. "The double-ITCZ bias in CMIP3, CMIP5, and CMIP6 models based on annual mean precipitation". In: *Geophysical Research Letters* 47.8 (2020), e2020GL087232.

[15] H. Tsujino et al. "Evaluation of global ocean–sea-ice model simulations based on the experimental protocols of the Ocean model Intercomparison Project phase 2 (OMIP-2)". In: *Geoscientific Model Development* 13.8 (2020), pp. 3643–3708. DOI: 10.5194/gmd-13-3643-2020. URL: https://gmd.copernicus.org/articles/13/3643/2020/.

[16] E. P. Chassignet et al. "Impact of horizontal resolution on global ocean–sea ice model simulations based on the experimental protocols of the Ocean Model Intercomparison Project phase 2 (OMIP-2)". In: *Geoscientific Model Development* 13.9 (2020), pp. 4595–4637. DOI: 10.5194/gmd-13-4595-2020. URL: https://gmd.copernicus.org/articles/13/4595/2020/.

[17] Erik Behrens. "The oceanic response to Greenland melting: the effect of increasing model resolution". en. PhD thesis. 2013. URL: https://macau.uni-kiel.de/receive/diss_mods_00013684.

[18] David Walters et al. "The Met Office Unified Model global atmosphere 7.0/7.1 and JULES global land 7.0 configurations". In: *Geoscientific Model Development* 12.5 (2019), pp. 1909–1963.

[19] Nigel Wood et al. "An inherently mass-conserving semi-implicit semi-Lagrangian discretization of the deep-atmosphere global non-hydrostatic equations". In: *Quarterly Journal of the Royal Meteorological Society* 140.682 (2014), pp. 1505–1520. DOI: https://doi.org/10.1002/qj.2235. URL: https://rmets.onlinelibrary.wiley.com/doi/abs/10.1002/qj.2235.

[20] J. M. Edwards and A. Slingo. "Studies with a flexible new radiation code. I: Choosing a configuration for a large-scale model". In: *Quarterly Journal of the Royal Meteorological Society* 122.531 (1996), pp. 689–719. DOI: https://doi.org/10.1002/qj.49712253107. URL: https://rmets.onlinelibrary.wiley.com/doi/abs/10.1002/qj.49712253107.

[21] D. Gregory and P. R. Rowntree. "A Mass Flux Convection Scheme with Representation of Cloud Ensemble Characteristics and Stability-Dependent Closure". In: *Monthly Weather Review* 118.7 (1990), pp. 1483–1506. DOI: 10.1175/1520-0493(1990)118<1483:AMFCSW>2.0.CO;2. URL: https://journals.ametsoc.org/view/journals/mwre/118/7/1520-0493_1990_118_1483_amfcsw_2_0_co_2.xml.

[22] AR Brown et al. "Upgrades to the boundary-layer scheme in the Met Office numerical weather prediction model". In: *Boundary-Layer Meteorology* 128.1 (2008), pp. 117–132.

[23] A. T. Archibald et al. "Description and evaluation of the UKCA stratosphere–troposphere chemistry scheme (StratTrop vn 1.0) implemented in UKESM1". In: *Geoscientific Model Development* 13.3 (2020), pp. 1223–1266. DOI: 10.5194/gmd-13-1223-2020. URL: https://gmd.copernicus.org/articles/13/1223/2020/.

[24] Damian R. Wilson et al. "PC2: A prognostic cloud fraction and condensation scheme. I: Scheme description". In: *Quarterly Journal of the Royal Meteorological Society* 134.637 (Oct. 2008), pp. 2093–2107. DOI: 10.1002/qj.333. URL: https://doi.org/10.1002%5C%2Fqj.333.

[25] Damian R Wilsön et al. "PC2: A prognostic cloud fraction and condensation scheme. II: Climate model simulations". In: *Quarterly Journal of the Royal Meteorological Society* 134.637 (Oct. 2008), pp. 2109–2125. DOI: 10.1002/qj.332. URL: https://doi.org/10.1002%2Fqj.332.

[26] Andrew Brown et al. "Unified Modeling and Prediction of Weather and Climate: A 25-Year Journey". In: *Bulletin of the American Meteorological Society* 93.12 (2012), pp. 1865–1877. DOI: 10.1175/BAMS-D-12-00018.1. URL: https://journals.ametsoc.org/view/journals/bams/93/12/bams-d-12-00018.1.xml.

[27] Madec Gurvan et al. *NEMO ocean engine*. Version v4.2. Mar. 2022. DOI: 10.5281/zenodo.6334656. URL: https://doi.org/10.5281/zenodo.6334656.

[28] A. Yool, E. E. Popova, and T. R. Anderson. "MEDUSA-2.0: an intermediate complexity biogeochemical model of the marine carbon cycle for climate change and ocean acidification studies". In: *Geoscientific Model Development* 6.5 (2013), pp. 1767–1811. DOI: 10.5194/gmd-6-1767-2013. URL: https://gmd.copernicus.org/articles/6/1767/2013/.

[29] Elizabeth Hunke et al. *CICE, The Los Alamos Sea Ice Model, Version 00*. May 2017. URL: https://www.osti.gov/biblio/1364126.

[30] D. Storkey et al. "UK Global Ocean GO6 and GO7: a traceable hierarchy of model resolutions". In: *Geoscientific Model Development* 11.8 (2018), pp. 3187–3213. DOI: 10.5194/gmd-11-3187-2018. URL: https://gmd.copernicus.org/articles/11/3187/2018/.

[31] A. Craig, S. Valcke, and L. Coquart. "Development and performance of a new version of the OASIS coupler, OASIS3-MCT_3.0". In: *Geoscientific Model Development* 10.9 (2017), pp. 3297–3308. DOI: 10.5194/gmd-10-3297-2017. URL: https://gmd.copernicus.org/articles/10/3297/2017/.

[32] Till Kuhlbrodt et al. "The Low-Resolution Version of HadGEM3 GC3.1: Development and Evaluation for Global Climate". In: *Journal of Advances in Modeling Earth Systems* 10.11 (2018), pp. 2865–2888. DOI: https://doi.org/10.1029/2018MS001370. URL: https://agupubs.onlinelibrary.wiley.com/doi/abs/10.1029/2018MS001370.

[33] Alistair A Sellar et al. "UKESM1: Description and evaluation of the UK Earth System Model". In: *Journal of Advances in Modeling Earth Systems* 11.12 (2019), pp. 4513–4558.

[34] Laurent Debreu, Christophe Vouland, and Eric Blayo. "AGRIF: Adaptive grid refinement in Fortran". In: *Computers & Geosciences* 34.1 (2008), pp. 8–13.

[35] Jie He et al. "Impact of Ocean Eddy Resolution on the Sensitivity of Precipitation to CO_2 Increase". In: *Geophysical Research Letters* 45.14 (2018), pp. 7194–7203. DOI: https://doi.org/10.1029/2018GL078235. URL: https://agupubs.onlinelibrary.wiley.com/doi/abs/10.1029/2018GL078235.

[36] Yongming Tang et al. *MOHC UKESM1.0-LL model output prepared for CMIP6 CMIP historical*. 2019. DOI: 10.22033/ESGF/CMIP6.6113. URL: https://doi.org/10.22033/ESGF/CMIP6.6113.

[37] Hans Hersbach et al. "The ERA5 global reanalysis". In: *Quarterly Journal of the Royal Meteorological Society* 146.730 (2020), pp. 1999–2049.

[38] Lisan Yu and Robert A. Weller. “Objectively Analyzed Air–Sea Heat Fluxes for the Global Ice-Free Oceans (1981–2005)”. In: *Bulletin of the American Meteorological Society* 88.4 (2007), pp. 527–540. DOI: 10.1175/BAMS-88-4-527. URL: https://journals.ametsoc.org/view/journals/bams/88/4/bams-88-4-527.xml.

[39] William B Rossow and Robert A Schiffer. “Advances in understanding clouds from ISCCP”. In: *Bulletin of the American Meteorological Society* 80.11 (1999), pp. 2261–2288.

[40] WB Rossow and EN Duenas. “The international satellite cloud climatology project (ISCCP) web site: An online resource for research”. In: *Bulletin of the American Meteorological Society* 85.2 (2004), pp. 167–172.

[41] Erik Behrens. *erikbehrens/NZESM1: First release of the NZESM (ocean+sea ice code)*. Version v1.0. 2020. DOI: 10.5281/zenodo.3873691. URL: https://doi.org/10.5281/zenodo.3873691.

[42] Simon A Good, Matthew J Martin, and Nick A Rayner. “EN4: Quality controlled ocean temperature and salinity profiles and monthly objective analyses with uncertainty estimates”. In: *Journal of Geophysical Research: Oceans* 118.12 (2013), pp. 6704–6716.

[43] Gavin A. Schmidt et al. “Practice and philosophy of climate model tuning across six US modeling centers”. In: *Geoscientific Model Development* 10.9 (Sept. 2017), pp. 3207–3223. DOI: 10.5194/gmd-10-3207-2017. URL: https://doi.org/10.5194%2Fgmd-10-3207-2017.

[44] Frédéric Hourdin et al. “The Art and Science of Climate Model Tuning”. In: *Bulletin of the American Meteorological Society* 98.3 (Mar. 2017), pp. 589–602. DOI: 10.1175/bams-d-15-00135.1. URL: https://doi.org/10.1175%5C%2Fbams-d-15-00135.1.

[45] Doug McNeall et al. “Correcting a bias in a climate model with an augmented emulator”. In: *Geoscientific Model Development* 13.5 (May 2020), pp. 2487–2509. DOI: 10.5194/gmd-13-2487-2020. URL: https://doi.org/10.5194%2Fgmd-13-2487-2020.

[46] Petr Pisoft et al. “Stratospheric contraction caused by increasing greenhouse gases”. In: *Environmental Research Letters* 16.6 (May 2021), p. 064038. DOI: 10.1088/1748-9326/abfe2b. URL: https://dx.doi.org/10.1088/1748-9326/abfe2b.

[47] Lingyun Meng et al. “Continuous rise of the tropopause in the Northern Hemisphere over 1980–2020”. In: *Science Advances* 7.45 (2021), eabi8065. DOI: 10.1126/sciadv.abi8065. URL: https://www.science.org/doi/abs/10.1126/sciadv.abi8065.

[48] Kimberley J Reid et al. “Extreme rainfall in New Zealand and its association with Atmospheric Rivers”. In: *Environmental Research Letters* 16.4 (Mar. 2021), p. 044012. DOI: 10.1088/1748-9326/abeae0. URL: https://dx.doi.org/10.1088/1748-9326/abeae0.

[49] Dudley B. Chelton, Michael G. Schlax, and Roger M. Samelson. “Global observations of nonlinear mesoscale eddies”. In: *Progress in Oceanography* 91.2 (2011), pp. 167–216. ISSN: 0079-6611. DOI: https://doi.org/10.1016/j.pocean.2011.01.002. URL: https://www.sciencedirect.com/science/article/pii/S0079661111000036.

[50] Pauli Virtanen et al. “SciPy 1.0: Fundamental Algorithms for Scientific Computing in Python”. In: *Nature Methods* 17 (2020), pp. 261–272. DOI: 10.1038/s41592-019-0686-2.

[51] A. Bodas-Salcedo et al. “COSP: Satellite simulation software for model assessment”. In: *Bulletin of the American Meteorological Society* 92.8 (2011), pp. 1023–1043. DOI: 10.1175/2011BAMS2856.1. URL: https://journals.ametsoc.org/view/journals/bams/92/8/2011bams2856_1.xml.

[52] Gerald G. Mace and Forrest J. Wrenn. “Evaluation of the Hydrometeor Layers in the East and West Pacific within ISCCP Cloud-Top Pressure–Optical Depth Bins Using Merged CloudSat and CALIPSO Data”. In: *Journal of Climate* 26.23 (2013), pp. 9429–9444. DOI: 10.1175/JCLI-D-12-00207.1. URL: https://journals.ametsoc.org/view/journals/clim/26/23/jcli-d-12-00207.1.xml.

[53] Hideaki Kawai, Tsuyoshi Koshiro, and Mark J. Webb. “Interpretation of Factors Controlling Low Cloud Cover and Low Cloud Feedback Using a Unified Predictive Index”. In: *Journal of Climate* 30.22 (Nov. 2017), pp. 9119–9131. DOI: 10.1175/jcli-d-16-0825.1. URL: https://doi.org/10.1175%5C%2Fjcli-d-16-0825.1.

[54] Irina Mahlstein, Peter R. Gent, and Susan Solomon. “Historical Antarctic mean sea ice area, sea ice trends, and winds in CMIP5 simulations”. In: *Journal of Geophysical Research: Atmospheres* 118.11 (2013), pp. 5105–5110. DOI: https://doi.org/10.1002/jgrd.50443. URL: https://agupubs.onlinelibrary.wiley.com/doi/abs/10.1002/jgrd.50443.

[55] R. Kwok and D. A. Rothrock. “Decline in Arctic sea ice thickness from submarine and ICESat records: 1958–2008”. In: *Geophysical Research Letters* 36.15 (2009). DOI: https://doi.org/10.1029/2009GL039035. URL: https://agupubs.onlinelibrary.wiley.com/doi/abs/10.1029/2009GL039035.

[56] Viktor Sebestyén, Tímea Czvetkó, and János Abonyi. “The Applicability of Big Data in Climate Change Research: The Importance of System of Systems Thinking”. In: *Frontiers in Environmental Science* 9 (2021). ISSN: 2296-665X. DOI: 10.3389/fenvs.2021.619092. URL: https://www.frontiersin.org/articles/10.3389/fenvs.2021.619092.

[57] D. Ackerley et al. “Regional climate modelling in New Zealand: Comparison to gridded and satellite observations”. In: *Weather and Climate* 32.1 (2012), pp. 3–22. ISSN: 01115499. URL: http://www.jstor.org/stable/26169722 (visited on 02/06/2023).